Annales Societatis Geologorum Poloniae (2022), vol. 92: 295–312 doi: https://doi.org/10.14241/asgp.2022.09

TERRIGENOUS ORGANIC MATTER AND FORMATION OF SIDERITE IN THE BATHONIAN ORE-BEARING CLAY FORMATION AT GNASZYN, POLAND – A PETROCHEMICAL STUDY

Kacper LIS[1,*], Piotr WOJTULEK[1], Grzegorz LIS[1] & Iwona JELONEK[2]

[1] *University of Wrocław, The Institute of Geological Sciences, pl. Maksa Borna 9, 50-204 Wrocław, Poland; e-mails: kacper.lis@uwr.edu.pl, piotr.wojtulek@uwr.edu.pl, grzegorz.lis@uwr.edu.pl*
[2] *University of Silesia, The Institute of Earth Sciences, ul. Będzińska 60, 41-200 Sosnowiec, Poland; email: iwona.jelonek@us.edu.pl*
** Corresponding author*

Lis, K., Wojtulek, P., Lis, G. & Jelonek, I., 2022. Terrigenous organic matter and formation of siderite in the Bathonian Ore-Bearing Clay Formation at Gnaszyn, Poland – a petrochemical study. *Annales Societatis Geologorum Poloniae*, 92: 295–312.

Abstract: The Bathonian Ore-Bearing Clay Formation, outcropping in the Gnaszyn open-pit mine at Częstochowa (Poland), includes several horizons of abundant iron carbonate concretions. The cores of the concretionary bodies commonly contain organic matter (OM), dominated by fragments of wood. These organic particles usually display well-preserved primary structures and occur rarely as more deformed and/or completely degraded fragments. Their original structures are frequently replaced by or filled with secondary mineralization, mostly represented by pyrite. The maceral composition of the OM of the wood fragments is dominated by huminite with subordinate inertinite and resinite. Vitrinite reflectance analyses revealed values lower than 0.45%. The total organic carbon content (TOC) displayed variable results between 2% and 18%. Rock-Eval analyses revealed low amounts of hydrogen (< 45 mg HC/g TOC) and relatively high amounts of oxygen (up to 136 mg CO_2/g TOC). Analysed samples contained small quantities of free hydrocarbons (S1 peak < 0.26 mg HC/g rock) as well as hydrocarbons, generated during pyrolysis (S2 peak < 7.05 mg HC/g rock). These features are characteristic for immature type IV kerogen of terrigenous origin. However, the maceral composition and frequent occurrence of siderite affecting the Rock-Eval parameters may indicate that the original kerogen belonged to type III. According to previous authors, the OM of terrigenous origin was delivered to well-oxygenated water of the palaeo-basin in the Częstochowa area. The present data indicate that intensive biodegradation of this OM at shallow burial depleted the oxygen supply within the sediment, driving the pore water into dys- or anoxic conditions. The activity of microorganisms in reducing iron and/or sulphates became the dominant biodegradation reaction, introducing Fe^{2+} and HCO_3^- ions into the system. Negative $\delta^{13}C$ values in the cortex of the concretions analysed indicate that the bicarbonate consumed in siderite precipitation was supplied by this microbial activity. The reducing microenvironments developed in the sediment and wood fragments acted as nucleation sites for siderite precipitation.

Key words: Organic matter, kerogen, siderite concretions, microbial decay, Jurassic.

Manuscript received 13 October 2021, accepted 17 August 2022

INTRODUCTION

The presence of concretionary bodies in sedimentary formations is a distinctive phenomenon, which has attracted the attention of researchers for a long time. Around the beginning of the 20th century, many scientists documented the occurrence of concretionary bodies of different types (Daly, 1900; Bassler, 1908; Richardson, 1919; Tarr, 1921). As concretions might have been formed in many distinct environments, various hypotheses about the origin of these structures were presented. Concretionary bodies can be found in marine as well as in terrestrial environments in almost every kind of sedimentary rock: clays, sands and sandstones, limestones and volcanoclastics (Sellés-Martínez, 1996). They usually occur along particular horizons, each representing a specific record of diagenetic and/or sedimentary palaeoconditions (Coleman and Raiswell, 1993; Bojanowski *et al*., 2014). Sellés-Martínez (1996) created a classification of concretionary bodies, based on morphological, mineralogical, and genetic data. According to this

classification, one specific type of concretionary body is defined as concretions. These rock structures are usually spheroidal or flattened and ellipsoidal in shape. Concretions are formed as a result of the precipitation of authigenic material in pore spaces, which leads to cementation and incorporation of the host sediments (Sellés-Martínez, 1996; Raiswell and Fisher, 2000). Most of the concretions recognized are carbonate ones (Gautier, 1982; Blome and Albert, 1985; Mozley, 1996; Majewski, 2000; Zatoń *et al*., 2011; Bojanowski and Clarkson, 2012). This work presents the results of analyses of siderite concretions from the Bathonian Ore-Bearing Clay Formation at Gnaszyn, with particular attention to wood fragments in the cores of concretions and the conditions of their formation.

Iron carbonate (siderite) concretions usually are associated with early-diagenetic, reducing conditions (Majewski, 2000; Witkowska, 2012; Cotroneo *et al*., 2016). A relevant factor in their formation is commonly the presence of marine or terrestrial, organic matter (Blome and Albert, 1985; Sellés-Martínez, 1996; Janssen *et al*., 2022). The biodegradation of organic matter in reducing environments with minimal oxygen content can be carried out by microorganisms reducing iron and sulphates or by methanogenetic processes (Mozley and Carothers, 1992; Coleman *et al*., 1993; Bojanowski and Clarkson, 2012). Therefore, Fe^{2+} and HCO_3^- ions can be delivered into the system, which enables siderite precipitation under appropriate pH conditions (Roberts *et al.*, 2013; Lin *et al.*, 2020). Iron carbonate concretions commonly contain well-preserved, marine or terrestrial, organic particles (Blome and Albert, 1985; Marynowski *et al*., 2007; Cotroneo *et al*., 2016). This indicates the preferential growth of concretions around large, organic fragments. The cementation of organic remains by siderite protects them from the continued influence of diagenetic conditions and further biodegradation (Sellés-Martínez, 1996).

Multiple horizons of iron carbonate concretions were recognized in the Middle Jurassic clay formations, outcropping in the Częstochowa area (Poland), known as the Ore-Bearing Clay Formation. They were examined for mineralogical, palaeontological and palaeoenvironmental data by numerous authors (e.g., Różycki, 1953; Majewski, 2000; Marynowski *et al.*, 2007; Witkowska, 2012). These concretions commonly contain organic particles of higher plants showing different degrees of preservation (Majewski, 2000; Marynowski *et al*., 2007). In this paper, the present authors discuss in detail the mode of occurrence and properties of wood fragments, enclosed in siderite concretions in the Bathonian Ore-Bearing Clay Formation at the Gnaszyn Mine (Częstochowa, Poland). This clay-pit offers the possibility of investigation concretions that occur in horizons at various levels in the clay formation. Organic fragments occurring in the concretions permit the determination of their conditions of formation (Sellés-Martínez, 1996). Thus, the present authors here describe the mineralogical characteristics of the Gnaszyn iron carbonate concretions and present new data (petrographic and chemical) on the organic matter from the wood fragments. The aim of this account is to determine the conditions of formation of siderite concretions at the Gnaszyn Mine, with a focus on the early diagenetic processes, responsible for siderite precipitation, according to the current state of knowledge.

ARCHITECTURE OF THE CRACOW-SILESIA MONOCLINE

An open-pit mine of ceramic clay, Gnaszyn, is located in the Cracow-Silesia monocline (CSM), a part of the Polish Basin. During the Mesozoic era, this NW-SE-extended palaeo-basin covered almost the entire area of the current Polish Lowlands (Feldman-Olszewska, 1997). The central part of the Polish Basin, the Mid-Polish Trough, was an area subjected to a high rate of subsidence, leading to the deposition of a significant thickness of the Mesozoic sedimentary rocks (Feldman-Olszewska, 1997). The Jurassic rock formations of the Polish Basin were deposited in a marine regime. The thickness of its marine rock sequence varies between 300 m in distal regions of the Polish Basin and 1,000 m in the Mid-Polish Trough (Dayczak-Calikowska, 1997; Leonowicz, 2016). The Middle Jurassic evolution of the Polish Basin started in the Early Aalenian with the Tethys Ocean transgression. Until the end of the Bathonian, the connection with Tethys waters had a significant influence on eustatic changes in the basin, which achieved its maximum extension during the Late Bathonian (Dayczak-Calikowska, 1997).

The area of the CSM constitutes the southern part of the Polish Basin. The CSM comprises the Lower, Middle, and Upper Jurassic rocks, which dip towards the NE at several degrees (Feldman-Olszewska *et al*., 2017). The CSM comprises two regions differing in their tectonic structure (Fig. 1). The southern Kraków-Zawiercie area is characterized by its complicated tectonic structure, due to the presence of numerous faults, elongated mostly in a W-E direction. The northern part of the CSM is the Częstochowa area, the tectonic structure of which is rather regular and displays only a few major faults, trending in a NE direction. The Jurassic rock sequences in both regions are similar. The Lower Jurassic formations include Pliensbachian and Toarcian rocks, which are represented by sandy deposits, locally intercalated with sandstones and mudstones (Fig. 2). These formations occur only in the northern region of the CSM, extending in a NW direction between Zawiercie and Wieluń. The Middle Jurassic rocks appear in both, southern and northern regions. They are dominated by thick clay formations, known as the Ore-Bearing Clay Formation (Dayczak-Calikowska and Kopik, 1973; Majewski, 2000; Matyja and Wierzbowski, 2000). In the CSM, the thickness of the Middle Jurassic rocks increases towards the NW, reaching up to 300 m in the Częstochowa area (Stupnicka and Stempień-Sałek, 2016; Feldman-Olszewska *et al*., 2017). The Upper Jurassic sedimentary rocks are of widespread occurrence in the CSM and include a very thick sequence of massive limestones and microbial-sponge bioherms (Wierzbowski, 2015; Stupnicka and Stempień-Sałek, 2016). They were deposited in the Tethys Ocean, the opening of which was accompanied by the formation of its northern shelf in the CSM area (Kutek, 1994; Leonowicz, 2016).

The Gnaszyn claypit

The Gnaszyn Mine is located in the Częstochowa region. The Middle to Upper Jurassic marine sequence of

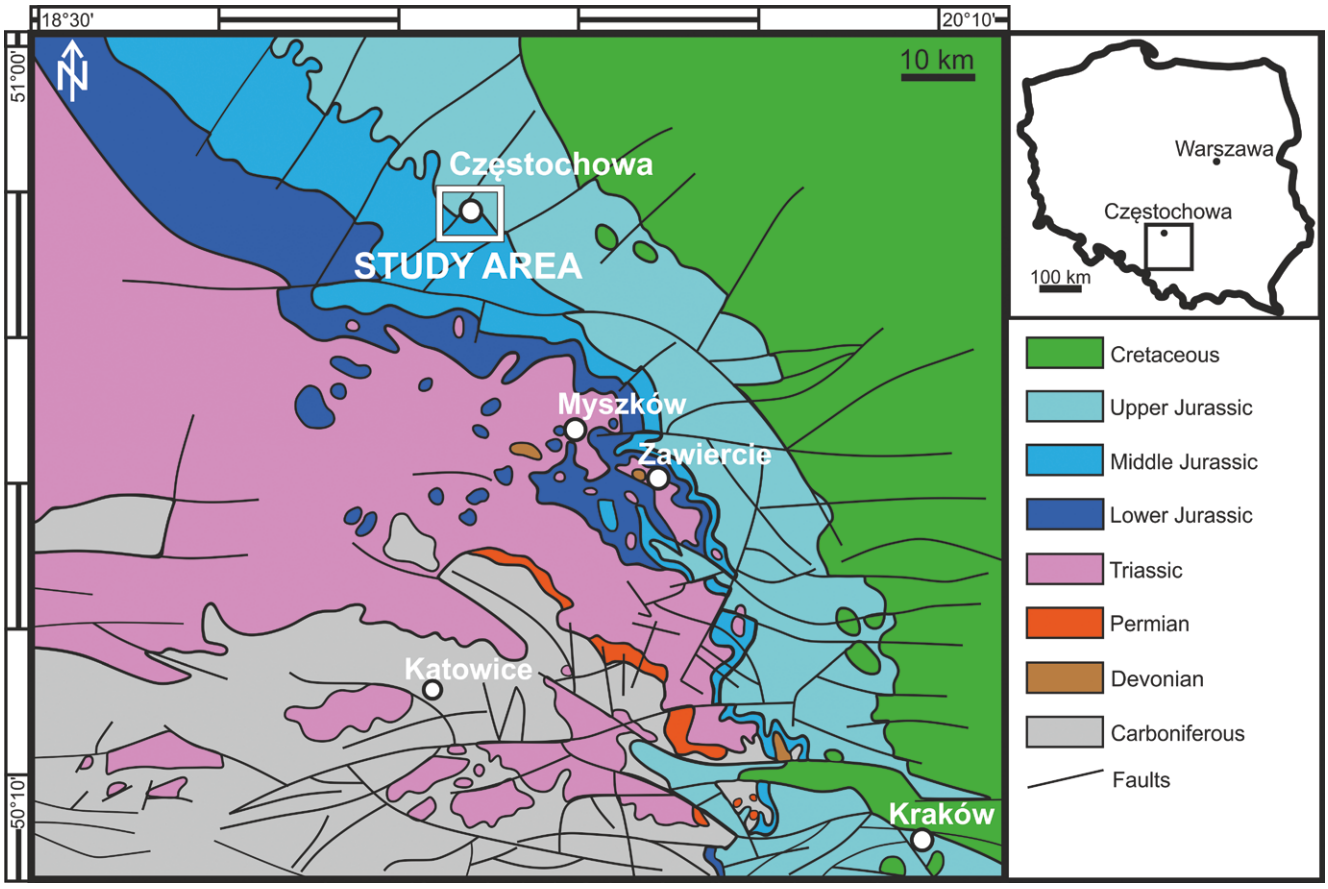

Fig. 1. General geological map of the Cracow – Silesian Monocline without Cenozoic cover (after Dadlez *et al.*, 2000).

sedimentary rocks of the Gnaszyn area comprises the following rock formations (Fig. 2):

1. The Aalenian and Lower Bajocian sands and gravels, up to 40 m thick and outcropping mainly in the northern part of the CSM, are associated with the beginning of marine transgression in the Częstochowa area (Dayczak-Calikowska and Kopik, 1973; Haisig, 2011; Stupnicka and Stempień-Sałek, 2016).
2. The Upper Bajocian consists of dark shales with siderite concretions, up to 100 m thick (the Ore-Bearing Clay Formation).
3. The Bathonian dark shales, sandy clays, and mudstones with siderite concretions (the Ore-Bearing Clay Formation), up to 140 m thick, were deposited in a deeper-water siliciclastic-shelf sub-system (Feldman-Olszewska, 1997; Haisig and Wilanowski, 2008; Haisig, 2011; Stupnicka and Stempień-Sałek, 2016).
4. The Callovian sandy and crinoidal limestones, up to 25 m thick, involve the Middle-Upper Jurassic boundary in the Polish Jura Chain that is often defined by nodular beds, condensed sequences and stromatolites, up to 10 cm thick, representing deposits of a shallower carbonate-clastic-shelf system (Różycki, 1953; Feldman-Olszewska, 1997; Dembicz and Praszkier, 2003; Wierzbowski *et al.*, 2009).
5. The Oxfordian, divided into two formations, (a) the Lower and Middle Oxfordian consist of thin-bedded limestones, marls, and spongy limestones up to 150 m thick, deposited in the northern shelf of the Tethys Ocean (Kutek, 1994); and (b) the Upper Oxfordian bedded limestones and massive limestones, formed from microbial-sponge bioherms. Their thickness reaches as much as 400 m and they form most of the Polish Jura Chain rocks (Haisig, 2011; Wierzbowski, 2015; Stupnicka and Stempień-Sałek, 2016; Feldman-Olszewska *et al.,* 2017).

The Ore-Bearing Clay Formation

The Middle Jurassic clays of the Polish Jura Chain belong to the Ore-Bearing Clay Formation and were formed between the Late Bajocian (*Garantiana* ammonite zone) and the end of the Bathonian (*Discus* ammonite zone; Matyja and Wierzbowski 2003; Leonowicz, 2015a). The Lower, Middle and Upper Bathonian sediments, occurring in the profile of the Gnaszyn Mine, are mainly silty clays and/or clayey silts (Gedl *et al.*, 2012; Leonowicz, 2015a). The entire profile of the formation in the Częstochowa area includes ubiquitous siderite concretions and horizons with an iron content of up to 35% (Osika and Cieśla, 1990). Therefore, until the middle of the 20th century, the Ore-Bearing Clay Formation was considered as one of the most significant sources of iron for Polish industry (Szczepańska and Witkowska, 2007). Iron mining in the Częstochowa region came to an end in 1982 when the last functioning mine was shut down (Ratajczak and Korona, 2000).

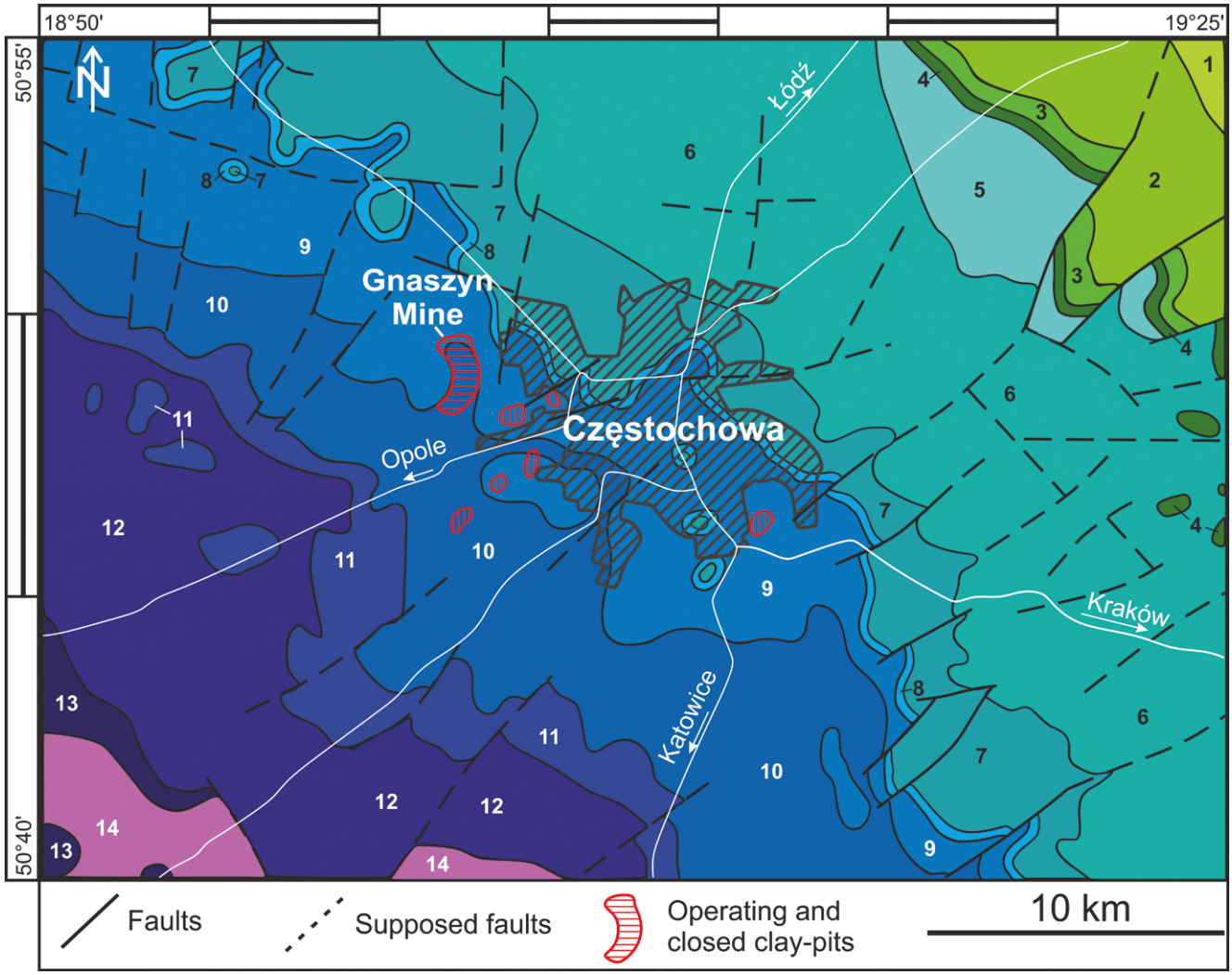

Fig. 2. Geological map of Gnaszyn Mine area, after Haisig and Wilanowski (2008) and Haisig (2011).
Legend: 1 – Maastrichtian marls; 2 – Campanian marls and limestones; 3 – Cenomanian-Santonian sandstones and limestones; 4 – Albian glauconite sandstones; 5 – Oxfordian-Kimmeridgian limestones and marls; 6 – Oxfordian massive and chalk limestones; 7 – Oxfordian bedded and massive limestones; 8 – Callovian sandy limestones; 9 – Bathonian clays with siderite concretions; 10 – Bajocian clays with siderite concretions; 11 – Aalenian-Bajocian sands; 12 – Toarcian sand and, sandstones; 13 – Pliensbachian sands, gravels; 14 – Upper Triassic clays and limestones.

The Ore-Bearing Clay Formation was formed in the marginal part of the Polish Basin, in its relatively shallow part, reaching up to a few tens of metres in thickness. Since the Late Bajocian, the Częstochowa area became covered by relatively shallow epicratonic sea, which was a part of a higher-order structure – the Polish Basin. The Bathonian transgression induced further extension of the Polish Basin and partial flooding of the lands surrounding the Częstochowa area. These basins developed under the Tethys Ocean regime, which also produced the Middle Jurassic transgressive pulses (Pieńkowski *et al*., 2008). The Ore-Bearing Clay Formation in the Gnaszyn Mine was deposited in a lower offshore to offshore transition zone, periodically passing to a distal lower shoreface (Leonowicz, 2015a, 2015b). These sediments resulted from the 7 Late Bajocian to Late Bathonian transgressive-regressive cycles that deposited fine-grained terrigenous material (Feldman-Olszewska, 1997; Leonowicz, 2015a). Other important factors affecting sedimentation in this basin were storm events and bottom-currents (Leonowicz, 2015b). Episodes of high-energy conditions caused the transport of fine- and coarse-grained material towards the basin. They affected also relatively unconsolidated sediment from the bottom, leading to erosion, exhumation, and redeposition of material (Leonowicz, 2015a, 2016). Szczepanik *et al*. (2007) and Zatoń *et al*. (2009) conducted geochemical environmental analyses in order to determine the redox conditions in basin waters during deposition of clays at the Gnaszyn Mine. Their analytical results, which included TOC/S, Ni/Co, V/Cr, U/Th, (Cu + Mo)/Zn ratios, content of authigenic uranium and TOC-Fe-S relationship, indicated that the Ore-Bearing Clay Formation was deposited under oxygenated bottom-water conditions.

SAMPLES AND METHODS

Samples

The profile of the ore-bearing clays comprises numerous horizons with siderite concretions. In the Gnaszyn Mine (50°48'15.4"N, 19°02'20.9"E), there are 7 horizons in sequence from N to T (N, O, P, Q, R, S, T; Matyja and Wierzbowski, 2003; Gedl *et al.*, 2012). The fieldwork of the present authors in the Gnaszyn Mine revealed the occurrence of three main iron carbonate concretion types: (1) mostly flattened concretions with an irregular shape, containing fragments of terrestrial plants; (2) spheroidal concretions with common septarian structures; and (3) small concretions, up to 7 cm in diameter, without macroscopically discernible organic matter, often containing sphalerite or galena in the concretion core. For the purpose of this study, the authors chose only the first type of concretion, containing wood fragments in the core. Eight concretions were sampled from horizon P of the Ore-Bearing Clay Formation at the Gnaszyn Mine. These horizons are classified as being Middle Bathonian in age, referable to the *Morissi* ammonite zone (Matyja and Wierzbowski, 2003; Gedl *et al.*, 2012). The concretions sampled are mostly elongated and their long dimensions are between 20 and 35 cm (Fig. 3). Each of them contains fragments of wood. These organic particles are in the central part of the concretions (cores) and are surrounded by a sideritic matrix.

Analyses of organic matter involved only samples of wood fragments from the cores of the concretions. Samples KL01, KL03, KL04, and KL06 containing abundant organic matter were selected for sub-sampling; wood fragment aliquots were extracted mechanically and separated for physicochemical analyses and petrographic observations. Thin sections were prepared from samples KL05 and KL07, which displayed well-preserved wood structures and the boundary between the organic matter and the siderite host rock. Deformed organic particles from samples KL01 and KL04 were chosen for pulverizing for Rock-Eval procedures. The results obtained in this project are presented as tables in electronic supplementary material (Appendix 1),

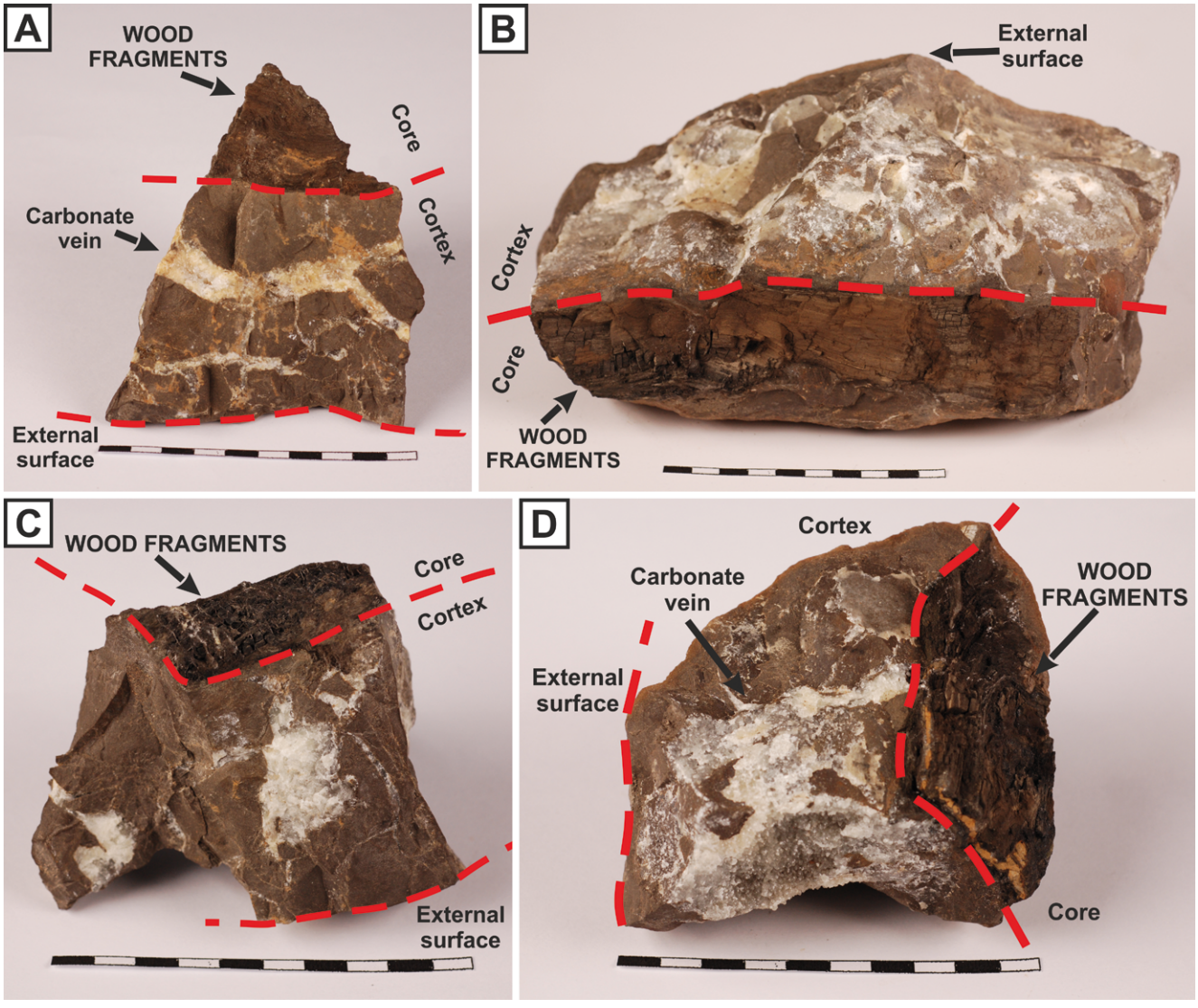

Fig. 3. Fragments of siderite concretions with wood fragments from the Gnaszyn Mine. **A.** Sample KL01, **B.** Sample KL04, **C.** Sample KL02, **D**. Sample KL03.

available online. The supplementary data also contain the results of the physicochemical analyses, conducted at the Department of Solid Fuels Quality Assessment, Central Mining Research Institute, in Katowice (determination of ash content, determination of volatiles, determination of total sulphur content, determination of total carbon content) as extended, additional information, concerning the properties of the organic matter from the core.

Electron probe microanalysis (EPMA)

Back-scattered electron (BSE) imaging and compositional analyses of minerals were conducted for carbon-coated thin sections of two samples of siderite concretions containing wood fragments (KL05 and KL07). The measurements were performed using a Cameca SX Five FE electron probe micro-analyser at the Faculty of Geology, University of Warsaw, Poland. Analytical conditions included an acceleration voltage of 15 kV, a beam current of 10 nA, and a beam size of 10 μm for siderite and 1 μm for pyrite (see Supplementary Table S1 for further details). The PAP correction procedure (Pouchou and Pichoir, 1984) was applied.

Rock-Eval analyses

The Rock-Eval (RE) analyses were conducted using the Rock-Eval 6 Turbo Vinci Technologies at the Polish Geological Institute – National Research Institute, in Warsaw, Poland. Samples for the analyses were extracted from siderite concretions KL01 and KL04. Wood fragments were pulverized in an agate mortar, then five sub-samples (weight between 79.8 mg and 107.7 mg) were taken for the RE analyses. In this study, a basic method of RE 6 was used, as described by Behar *et al.* (2001). Calculations of Oxygen Index were based on the formula: the CO_2 yield from the pyrolysis of organic particles (S3 peak) × 100 / TOC. The Hydrogen Index was determined according to the formula: yield of hydrocarbons generated during pyrolysis (S2 peak) × 100 / TOC. The final results included also Total Organic Carbon (TOC): computed by adding pyrolyzed carbon (PC) and residual carbon (RC); PI factor – Productivity Index: the free hydrocarbons measured in the sample (S1 peak) / (S1 + S2). The last factor analysed using RE was T_{max}, which is the maximum temperature of hydrocarbon generation.

Petrography and vitrinite reflectance analyses

Petrographic observations of thin sections of siderite containing wood fragments were conducted at the Institute of Mineralogy, Technische Universität *Bergakademie* Freiberg, Germany. Samples KL05 and KL07 were investigated using the Zeiss AxioCam Mrc 5 optical microscope (plane polarized light and reflected light observations). Axiovision software was used for image corrections (sharpness, optimization of colours).

Optical observations of organic matter from the core and maceral reflectance analyses were conducted for samples KL01, KL03, KL06. They were performed in UV and white reflected light at the Faculty of Earth Science of the University of Silesia, Poland, using the Zeiss Microscope AxioCam MRc 5. Reflectance analyses were carried out using the integrated system Zeiss AxioImager MSP400 CCD JM36375, equipped with a microphotometer. For analyses, fragments of organic matter were mechanically extracted from the cores of concretion samples. Samples were impregnated with synthetic resin, then polished. Petrographic observations were conducted with immersion oil (RI = 1.518) in monochromatic, unpolarized light (546 nm). Vitrinite reflectance was determined using a microphotometer that was calibrated with standards of known reflectance: Yttrium Aluminum Garnet (0.901), Gadolinium Gallium Garnet (1.718), and an optical black (0), which were also used for normalizations (Kruszewska and Dybová-Jachowicz, 1997; Hackley *et al.*, 2015). Analyses were conducted using the random reflectance method. A total of 180 measurements of light reflectance was prepared for samples KL01, KL03, KL06.

Carbon isotope analyses $\delta^{13}C$

Stable carbon isotope analysis ($\delta^{13}C$) was conducted using gaseous carbon dioxide, which was collected from the decomposition of iron carbonate with 103% H_3PO_4 at 25 °C (McCrea, 1950). The reaction vessel, with the powdered carbonate (up to 100 mg) in the tube and the phosphoric acid in the side arm, was evacuated and tipped to release the acid onto the carbonate. After the conversion into CO_2, the gas was expanded into the rest of the system and then frozen with liquid nitrogen cooling. The amount of carbon dioxide was measured using a manometer and transferred to mass spectrometer isotopic analyses (McCrea, 1950). The isotopic composition was measured by means of a FinniganMAT Delta mass spectrometer in the Laboratory of Isotope Geology and Geoecology, at the University of Wroclaw. The isotopic ratios of carbon in the analysed samples were normalized to the VPDB standard and the analytical error was ± 0.1‰.

RESULTS

Macroscopic observations

The concretions sampled at the Gnaszyn Mine are mostly 20–35 cm in diameter. Their structure is divided into the cortex, dominated by micritic siderite and dispersed siliciclastic material, and the core, occupied by wood fragments. The concretions display diverse shapes, mostly spheroidal and flattened or elongated ellipsoids. The last ones probably adopted the shapes of the wood fragments present in their cores. Organic matter occurs only in the central parts of the concretions (core) and is represented by individual fragments of terrestrial, higher plants. The wood fragments in each concretion have elongated shapes and are mostly 10–15 cm long and 5 cm wide (Fig. 3). Samples of the organic matter reveal a mostly well-preserved wood structure, but sometimes the structure is microscopically not visible. The wood fragments in the concretions are rather coherent and highly consolidated with their host concretions. The sideritic matrix (cortex), surrounding the organic matter

of the core, is frequently transected by calcite veins, up to 1 cm wide. Occasionally, wood fragments also are crossed by calcite veins, up to 1 mm wide (Fig. 3C). Sporadically, the marginal parts of concretions, as well as the wood in the core, display sulphide mineralization, represented by small-scale (up to 10 mm) occurrences of galena and sphalerite. The concretions sampled did not reveal traces of marine fossils, apart from scarce fragments of bivalve shells.

Microscopic observations and chemistry of minerals

EPMA measurements revealed that the cortex is composed of finely crystalline siderite, which cements dispersed siliciclastic material (e.g., quartz, feldspars, mica, and clay minerals) and framboidal pyrite (Fig. 4E, F). Small (up to 100 μm) and sparse accumulations of organic matter were also recognized within the sideritic cortex.

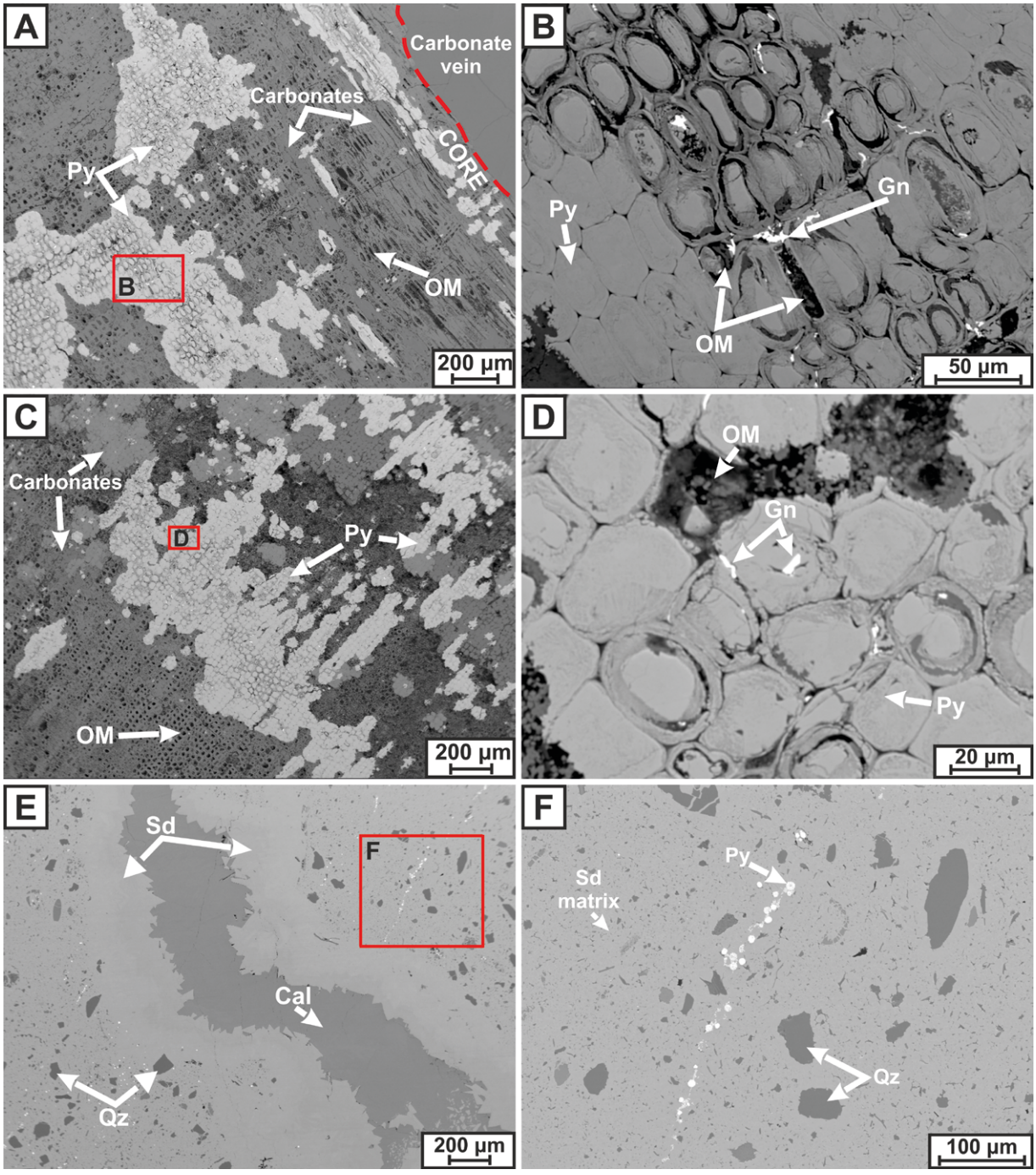

Fig. 4. Back-scattered electron (BSE) images of siderite concretions with wood fragments from the Gnaszyn clay-pit. **A–D**. Cores with well-preserved structures of wood cells. Organic matter occurs within the cell walls or fills the spaces between the cells. Original wood structures are substituted by carbonate mineralization: siderite and Fe-bearing calcite, and void-filling pyrite (sample KL05). **E–F**. Cortex without visible organic matter (sample KL07). **E**. Central part displays carbonate vein within cortex of concretion. Vein includes three stages of mineralization: older and younger sideritic stage, followed by the youngest, calcitic stage. **F**. Sideritic matrix, which cements fine-grained, siliciclastic material (quartz, feldspars, micas) from the cortex of concretion. Pyrite forms framboidal structures. Cal: calcite; Gn: Galena; OM: organic matter; Py: pyrite; Qz: quartz; Sd: siderite.

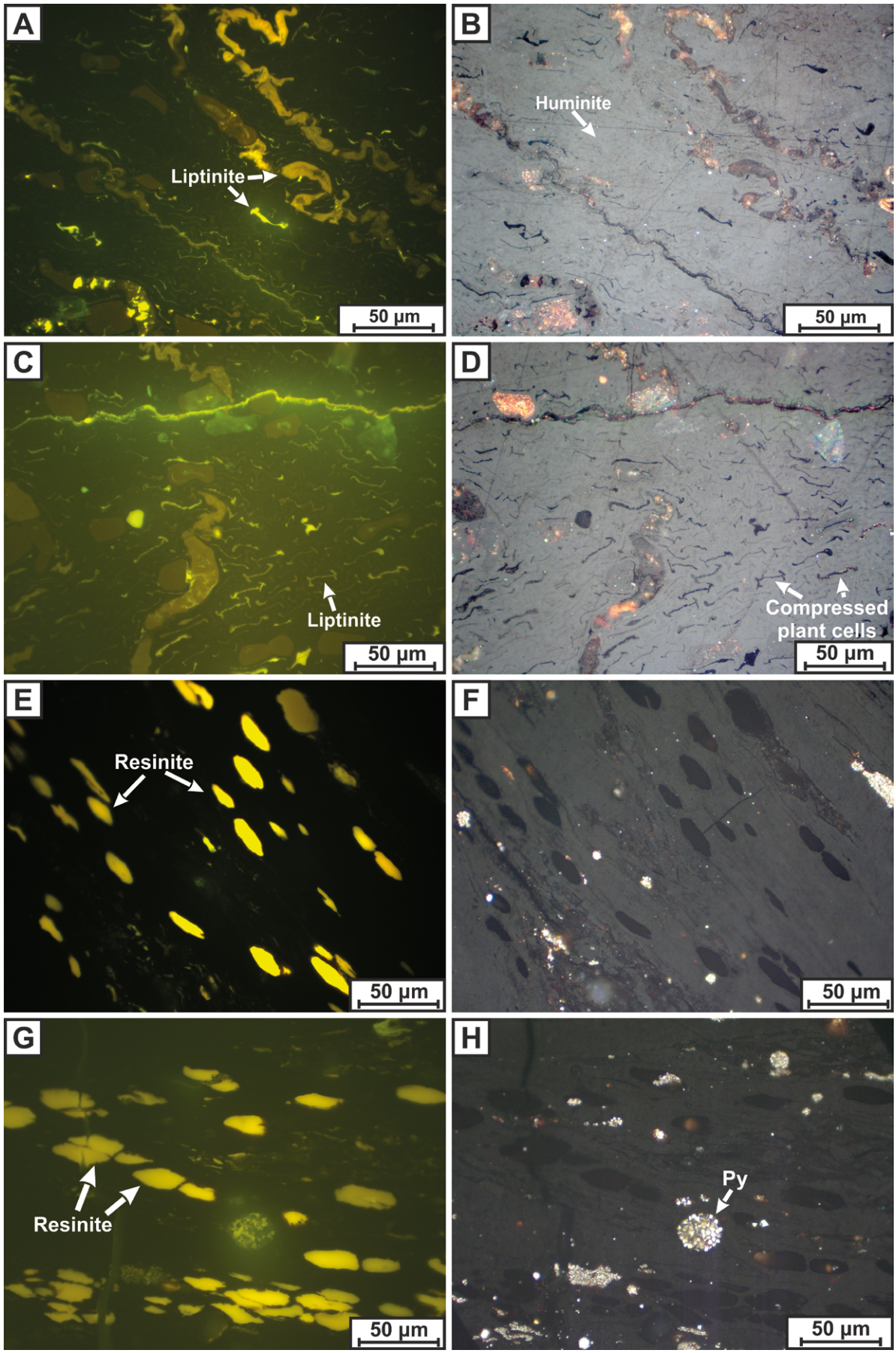

Fig. 5. UV and reflected light images of wood from the cores of concretions. **A–D**. Sample KL01, obliterated wood structure with compressed plant cells. Macerals dominated mostly by huminite and liptinite occurs in the form of elongated streaks. **E–H**. Sample KL03, undetectable, original wood structure with common, small (up to 50 µm), spherical bodies of resinite. Pyrite occurs as framboidal

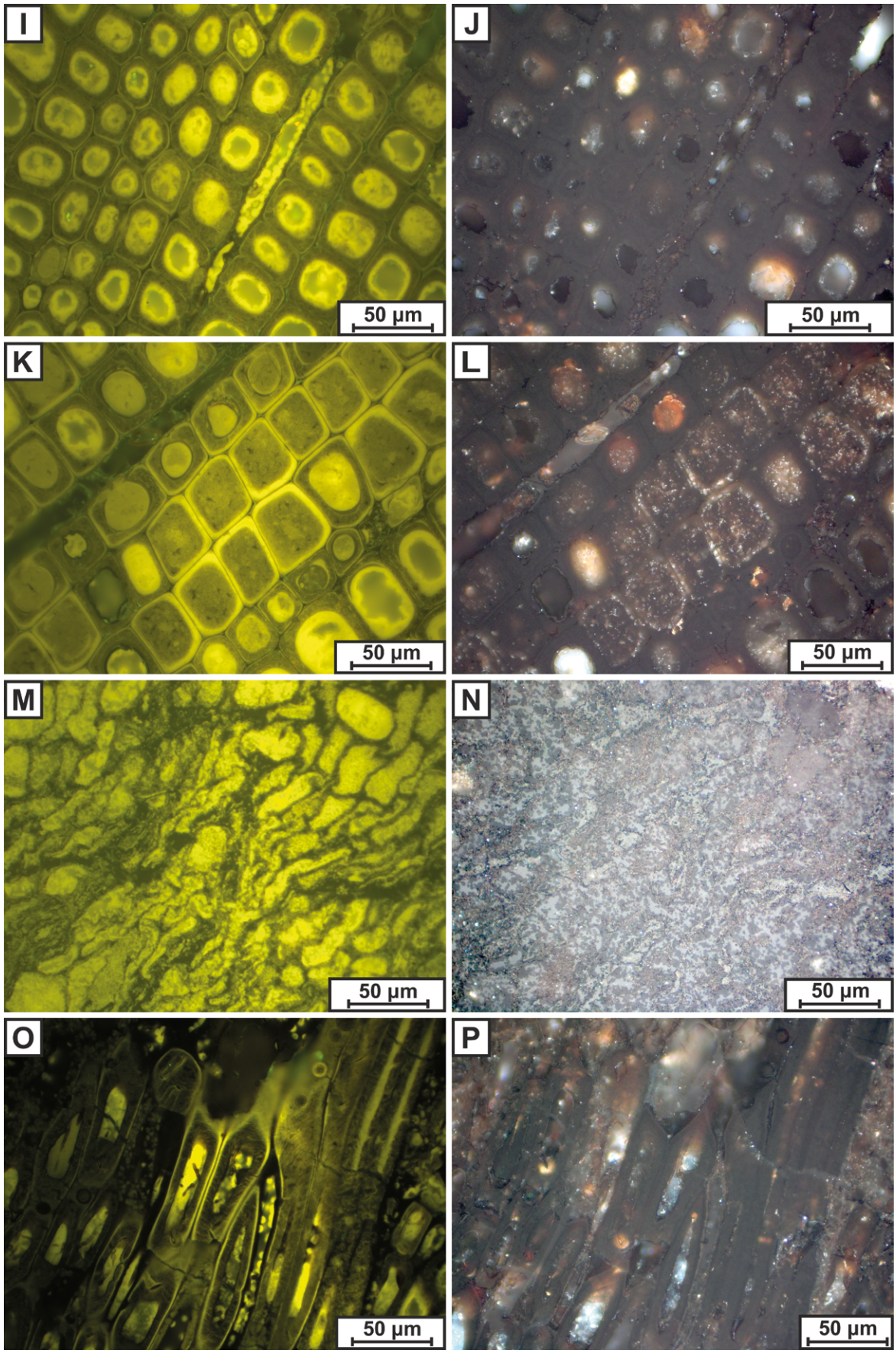

accumulations. **I–L** & **O–P**. Sample KL06, well-preserved wood structures, images O-P display cells cut along elongation. Cell interiors usually are filled with fluorescent mineral matter (carbonates represented by siderite and calcite) and pyrite. Organic matter occurs as thin layers within cell walls. **M–N**. Sample KL06, obliterated wood structure with intercalations of huminite and fluorescent mineral matter (carbonates). Py: pyrite.

The cores are occupied by relatively large wood fragments, mostly with well-preserved cellular wood structure. Original organic matter usually fills the cells or occurs within the cell walls (Fig. 4A, B). The parts with more biodegraded wood structure contain dispersed organic matter. Organic matter also coexists with siderite and Fe-bearing calcite, which fill voids or cement the cellular wood structures (Fig. 4A, C). These minerals also are found inside the cells. Apart from carbonates, there is also pyrite mineralization within the wood structures. Pyrite mostly occurs in a form of void-filling aggregates, replacing the original organic matter in the structures.

Both the core and the cortex are fractured and filled with coarsely crystalline carbonate material, including carbonate veins within the sideritic cortex (Fig. 4E). Three zones of mineralization can be distinguished within the vein: 1) the outer zone, containing mostly siderite, characterized by the highest Fe content, 2) the middle zone, also containing siderite, but with lower Fe and higher Ca content, and 3) the inner zone, composed of Fe-bearing calcite.

The fine-grained sideritic matrix contains 49.34–51.83 wt.% FeO, 2.92–5.77 wt.% CaO and 2.20–3.15 wt.% MgO (Supplementary Table S2). Some grains also display a slightly higher content of MnO (0.18–0.50 wt.%) and P_2O_5 (0.23–0.51 wt.%). The older sideritic mineralization of the carbonate veins (Fig. 4E) reveals lower amounts of FeO (48.62 wt.%) and higher CaO (6.06 wt.%). The CaO content in the younger sideritic stage increases (7.62 wt.%) and FeO content decreases (45.78 wt.%). Both the framboidal pyrite occurring in the matrix and the void-filling pyrite occurring in the wood structures contain 45.76–45.93 wt.% Fe and 52.32–53.88 wt.% of S, as well as 0.05–0.12 wt.% Co, 0.04–0.15 wt.% As, 0.1–0.17 wt.% Sn and do not show significant differences. The analyses also reveal trace amounts (<0.1 wt.%) of Pb and Cu.

The BSE and reflected light images show an often well-preserved, cellular wood structure; individual wood cells are for the most part only slightly deformed (Figs 4, 5I–L). However, microscopic observations revealed that some of the cells display flattened shapes (Fig. 5G, D, P). The maceral composition of the organic matter is complex: it varies, depending on the sample analysed. The organic matter in the wood fragments in the core is represented mainly by macerals in the huminite group. It appears as light-grey layers of textinite and as a more gelified form of ulminite. Textinite and ulminite analysed in UV light are black and opaque (Fig. 5A, C). These macerals usually were found within the more deformed wood cellular structures (Fig. 5B, D). Huminites also were recognized in the form of thin layers in well-preserved cell walls. Layers of macerals frequently are intercalated with siliciclastic material. Macerals belonging to the inertinite and liptinite groups occur subordinate. They are represented by complex inertinite detritic layers and small, spherical bodies of resinite (Fig. 5E, G).

Reflectance analyses

Reflectance analyses, conducted on macerals from the huminite group, gave variable results (Supplementary Tab. S3). The lowest values (~0.14%, n = 25) were measured on huminite layers from the cell walls of wood. Measurements on deformed cellular structures, probably represented by ulminite, gave an average value of 0.27% (n = 25). Analyses conducted on textinite displayed medium results of around 0.33% (n = 30). The highest reflectance measurements in the huminite group (0.35%, n = 25) were derived from small ulminite grains occurring inside the cells. Macerals from the inertinite group occur in dispersed layers, filling the spaces between deformed cellular structures (Fig. 5M, N). The reflectance of inertinites was slightly higher than that of huminites and gave average results of 0.35% (n = 25). The last of the macerals recognized – resinite, belonging to the liptinite group - occurs in greater amounts only in sample KL03 (Fig. 5E, G). It appears there as spherical and slightly elongated bodies, up to 50 μm in size. In white light, it is opaque but in UV light, it displays yellow fluorescence.

$\delta^{13}C$

Three analyses of stable carbon isotopes were conducted on samples KL01, KL02 and KL03. The sideritic material for analyses was collected from the cortex of concretions. The results obtained display values of -9.5‰, -9‰ and -7.8‰, respectively.

Chemical characterization of organic matter

The analysed wood fragments from the cores display mostly homogenous chemical properties. Only TOC values show large variability between 2% and 18% (Tab. 1). The carbon present in the organic matter consists mostly of residual carbon (RC), constituting 93% of the TOC,

Table 1

Physico-chemical parameters of organic matter from the core of the siderite concretions.

SAMPLE	S1	S2	T_{max}	HI	OI	OI CO	PI	TOC	RC (%)	PC (%)
KL01	0.04	0.93	428	13	76	-	0.04	5.90	95.25	4.75
KL03	0.13	1.36	414	33	98	43	0.08	4.17	92.27	7.43
KL04	0.12	7.05	412	45	66	-	0.02	14.61	93.29	6.70
KL05	0.04	0.39	412	19	136	54	0.10	2.00	92.00	8.00
KL06	0.26	6.84	420	38	106	41	0.04	18.07	92.09	7.91

whereas pyrolysable carbon (PC) amounts to 7%. Organic matter is characterized by very low amounts of free hydrocarbons (S1 peak), which do not exceed 0.26 mg HC/g rock. The yield of hydrocarbons generated during pyrolysis (S2 peak) is also poor: samples KL06 and KL04 displayed values of 6.84 and 7.05, respectively, while the other samples gave results lower than 1.36 mg HC/g rock.

The results for the Oxygen Index of the organic matter from the cores of the concretions are up to 136 mg CO_2/g TOC (averaging 96 mg CO_2/g TOC). The Hydrogen Index varies between 13 and 45 mg HC/g TOC (averaging 29 mg HC/g TOC; Tab. 1 and Fig. 6). The thermal maturity of organic matter was also estimated using the maximum temperature of hydrocarbons generation indicator, T_{max}. The T_{max} values for organic matter from Gnaszyn vary from 412 to 428 °C.

DISCUSSION

The observations of the present authors confirm that the organic matter in the cores of the analysed siderite concretions originated from the remnants of terrestrial higher plants, on the basis of the well-preserved, original wood structures observed in the samples (Figs 4, 5). According to Majewski (2000) and Cotroneo *et al.* (2016), iron carbonate concretions are usually formed at the stage of early diagenesis, usually to a depth of 10 m. The presence of undeformed wood cells from the concretion core could be evidence of early cementation during very shallow burial. The crystallization of siderite around the wood fragments formed a firm coating, which could have prevented deformation of the organic particles by compaction during increasing pressure of the overburden. Nonetheless, undeformed cells also could indicate brief exposure to oxygenated conditions, which prevented further decomposition of the organic matter. Oxygenated conditions influenced wood fragments mostly during fluvial transportation and shortly after deposition, at the bottom of the basin. Among the samples collected, there were also examples of wood fragments with obliterated or deformed cellular structure. As all the collected concretions occur within a single horizon, the authors assume that the wood samples with more obliterated structures have been affected by the same diagenetic conditions as the well-preserved ones. Hence, stronger deformation could be related to longer decay and residence in oxic conditions before siderite precipitation.

Amongst all of the recognized macerals from the Gnaszyn samples, the huminite group is the most common. Macerals belonging to this group originate from plant tissues and wood fragments, decomposed by humification and gelification processes (Kruszewska and Dybová-Jachowicz, 1997). Textinite usually occurs within the well-preserved wood cells and insignificantly modified structures. A higher degree of gelification of organic particles and obliterated tissue structure are related to the presence of ulminite. Diversity of transformation and decomposition between the samples probably originates from differences between wood fragments delivered to the basin. The duration of the exposure to oxidizing conditions on land and associated differences in the degree of decomposition of organic matter result in varying degrees of preservation. Shorter exposure favours preservation and the presence of textinite, whereas longer exposure favours decomposition and the presence of ulminite (Kruszewska and Dybová-Jachowicz, 1997). Sample KL03 reveals the presence of a maceral with yellow fluorescence, indicated as resinite of the liptinite group (Fig. 5E, G). Its occurrence is related to resins and essential oils from plant tissues. Resins and waxes are often well-preserved in different types of coal, because of their high tolerance of biochemical factors (Ceglarska-Stefańska, 1994).

The TOC content in wood fragments from the siderite concretions varies from 2% to 18%. Fresh organic matter from terrestrial higher plants usually contains approximately 50% carbon content (Lamlom and Savidge, 2003; Yeboah *et al.*, 2014). Such a noticeable decrease in carbon content in analysed wood samples supposedly is related to the loss of carbon, a process occurring during biodegradation of organic matter originating from the terrestrial higher plants, probably before or during burial. It also could be related to carbon dilution by carbonates and sulphides, in the post-depositional stage (Marynowski *et al.*, 2007). Carbon loss is compensated by a high ash content (non-organic mineral residue after combustion, Killops and Killops, 2005). A high ash content is confirmed by optical analyses, which reveal that the original structures of the wood debris usually are filled by sulphides and carbonates (Fig. 4A–D).

According to the OI *vs*. HI diagram, organic matter from the core of a siderite concretion was classified as kerogen type IV (Fig. 6). Generally, this type is considered to have multiple origins, but mainly terrestrial. It usually is highly biodegraded, oxygenated, and altered before the final deposition in sediment (McCarthy *et al.*, 2011; Peters *et al.*, 2012). During oxygenation, hydrogen is replaced by oxygen (Peters, 1986), which could be a reason for such low values of Hydrogen Index (13–45 mg HC/g TOC). Kerogen

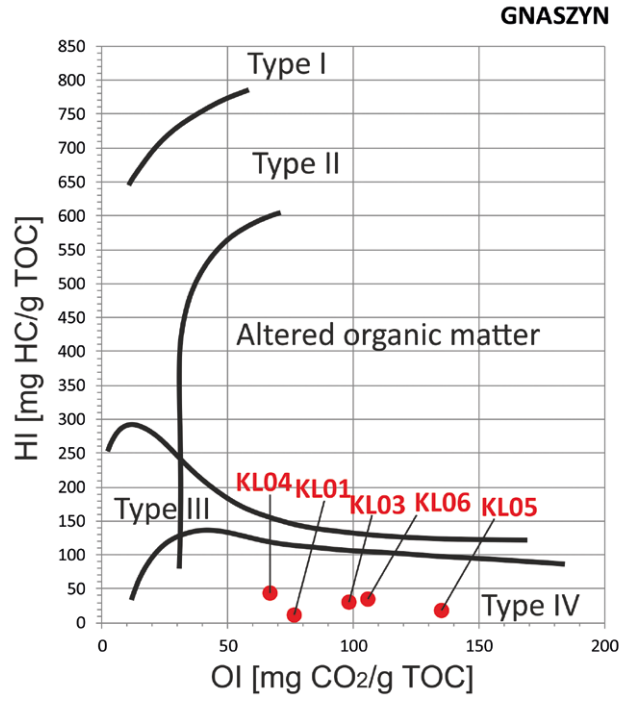

Fig. 6. Oxygen Index *vs*. Hydrogen Index ratios on a modified van Krevelen's classification diagram.

type IV often occurs in biodegraded wood material from the higher plants (Killops and Killops, 2005), comparable to the ones from the siderite concretions from the Gnaszyn Mine. Rock formations carrying this type of organic matter have no prospects for hydrocarbon exploration, since they can generate only insignificant amounts of aromatic hydrocarbons (Killops and Killops, 2005). Moreover, the presence of carbonates occurring with organic matter can influence the RE results. The most important in this case seems to be siderite, which is rather abundant around the organic matter. The decomposition of siderite starts during the pyrolysis stage and leads to the production of CO and CO_2 (Lafargue *et al.*, 1998). TOC and OI measurements are based on quantity of CO and CO_2 released during the pyrolysis of organic matter. It must be taken into account that the final values of TOC and OI can be overestimated as a result of CO and CO_2 from siderite decomposition driving the kerogen type into the kerogen IV window on the basis of the increased OI and decreased HI. HI decreases owing to siderite-derived CO and CO_2, both of which contribute to the TOC, calculated using RE parameters (Behar *et al.*, 2001). On the other hand, organic petrography observations (Fig. 5) reveal that the main maceral group observed in the cores of the siderite concretions belongs to the huminite group and inertinite particles appear only in trace amounts. As the organic petrography indicates kerogen type III on the basis of maceral composition and RE data indicate kerogen type IV, the organic matter from the Gnaszyn iron carbonate concretions could be either a mixture of types III and IV or more likely mainly type III, showing that RE parameters are affected by siderite thermal decomposition during measurement.

The Rock-Eval analyses separate measured TOC into pyrolysable and residual carbon. Residual carbon represents around 93% of the TOC and pyrolysable carbon the remaining 7%. It means that analysed organic matter from the wood fragments is dominated by organic components, which did not undergo pyrolysis. Residual carbon is a part of a highly condensed kerogen structure, which contains very small amounts of hydrogen (McCarthy *et al.*, 2011). Organic particles with such amounts of hydrogen usually are the products of transformations, caused by biodegradation, thermal degradation, and other processes leading to the decomposition of organic matter (Killops and Killops, 2005; McCarthy *et al.*, 2011). S1 peak measurements revealed a very low free hydrocarbon content in the organic matter analysed. A very low yield of S2 peaks means that the organic matter from the siderite concretions does not have the potential to generate hydrocarbons during further maturation. Source rocks, which yield the petroleum of oil and gas fields, achieve values of S1 and S2 peaks that are several times higher (Labus *et al.*, 2019).

Analyses of maceral reflectance show values lower than 0.45%. According to this, it can be assumed that organic matter from the cores of the siderite concretions is immature, since the maceral reflectance did not exceed 0.5% (Fig. 7; Alyousuf *et al.*, 2011). T_{max} measurements vary between 412–428 °C, which, in some cases, can be additional evidence for the immaturity of organic matter (Dembicki, 2017). However, it should be mentioned that the use of T_{max} in estimating thermal maturity is most reliable for kerogen type II, because of differences in the cracking kinetics among the other types of kerogens (Dellisanti *et al.*, 2010). The kerogen from siderite concretions was classified as immature organic matter. Results of the analyses conducted in this work revealed that the organic matter of Middle Jurassic age from the cores of the siderite concretions from the Gnaszyn Mine, does not have the potential for hydrocarbon generation, owing to very low hydrogen content in its structures and to thermal immaturity.

Apart from organic matter, the siderite concretions from the Gnaszyn open-pit also contain: siliciclastic material (quartz, feldspars, micas), carbonates (represented by calcite and siderite), and sulphides, which are dominated by pyrite. Pyrite creates mostly void-filling aggregates, which fill cell structures in the wood fragments. It also was recognized in smaller amounts in the form of spherical, framboidal structures, in the sideritic cortex (Fig. 4F). The occurrence of those structures at the Gnaszyn Mine already was confirmed by previous authors (Marynowski *et al.*, 2007; Zatoń *et al.*, 2008). The origin of pyrite is related to the occurrence of anoxic conditions in the sediment column. One of the transitional stages in framboidal pyrite formation is the transformation of mackinavite (FeS) into greigite (Fe_3S_4) via the addition of elemental sulphur. The progress of this conversion requires weakly reducing conditions, with minimal amounts of oxidants (Wilkin and Barnes, 1997; Zatoń *et al.*, 2008). In most of the non-stratified basins, such conditions occur usually at shallow depths below the sediment-water boundary. Previous analyses of the Ore-Bearing Clay Formation confirmed that the waters in the basin of the Częstochowa

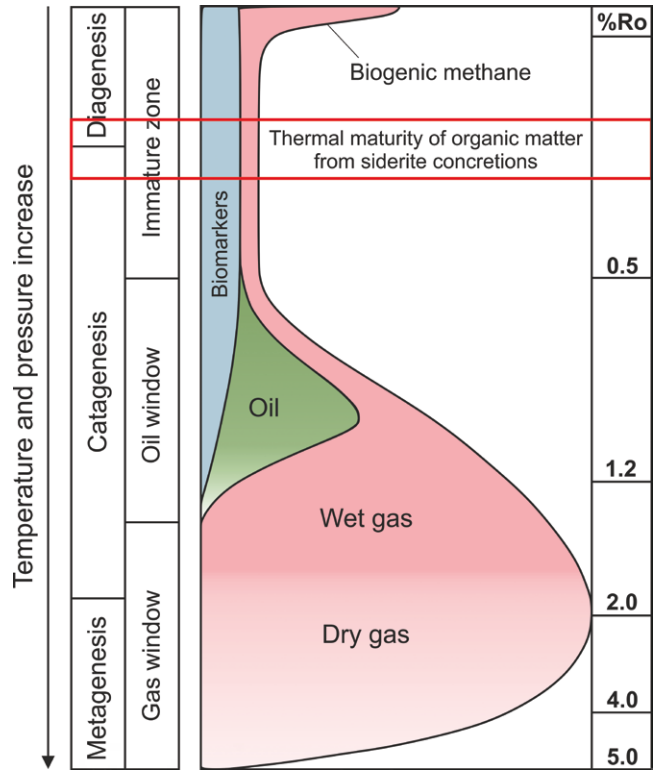

Fig. 7. Diagram of thermal transformation of kerogen by McCarthy *et al.* (2011) after Tissot *et al.* (1974) with $\%R_o$ values for vitrinite from siderite concretions from Gnaszyn Mine.

area were well-oxygenated (Szczepanik *et al*., 2007). Thus, it can be assumed that the formation of framboidal pyrite took place at rather shallow levels in a sediment column, under anoxic conditions.

The Bajocian and Bathonian clays at the Gnaszyn Mine reveal many sedimentary structures, including coarse-grained lenses, mud horizons, shell debris accumulations, and discrete cross-lamination, which indicate highly energetic events affecting the basin of the Częstochowa area. Those events disrupted the background sedimentation of clay material (Leonowicz, 2015a). Sedimentation in the palaeo-basin of the Gnaszyn area is classified as quiet from suspension, with highly-energetic episodes induced by common storm events, sea-level fluctuations, determined by transgressive-regressive cycles, shoreline variability, and bottom currents (Leonowicz, 2013, 2015a). All these processes influenced the sea-bottom and led to increased mixing of the basin waters, preventing anoxic or dysoxic conditions in the water column (Zatoń *et al.*, 2009; Leonowicz, 2015b).

Formation of siderite concretions

The analytical results, integrated with literature data, allowed the creation of a simplified model for formation of the siderite concretions in the Bathonian Ore-Bearing Clay Formation, in Częstochowa (Poland). This model takes into account the general palaeogeography of this region. The Bathonian basin of the Częstochowa area was a relatively shallow, epicratonic sea, on the southern border of the Polish Basin (Feldman-Olszewska, 1997). At that time, the Bohemian Massif and the Scandinavian Shield were the main sources of terrigenous material, as well as the organic matter delivered to the basin (Marynowski *et al.*, 2007). However, during the Middle Jurassic, the nearest emerged land was the Małopolska Land, which could have been a source of plant fragments for the Częstochowa basin (Leonowicz, 2016). However, no taxonomic analyses were performed, so the exact source area of plant remains cannot be defined. In the terrestrial environment, organic matter was transformed mainly by atmospheric weathering and decomposition by microorganisms. The RE data indicate kerogen type IV and thus potential oxygenation of organic matter during exposure and transport. On the other hand, the maceral composition indicates kerogen type III, with only small amounts of inertinite and thus a lack of significant oxygenation of the organic matter. Nonetheless, one should not exclude the possibility of at least partial decomposition of primary kerogen, owing to prolonged biodegradation on land. The time of exposure to atmospheric conditions could have exerted a significant influence on the degree of preservation and the generative potential of the organic matter analysed. Oxygenation also occurred during fluvial transport into the basin. At this stage, defragmentation of the larger wood fragments could have occurred, as well. After reaching the depositional area, wood fragments accumulated at the bottom of the basin. Although anoxic events occurred occasionally, for the most part the Bathonian basin of the Częstochowa area was well-oxygenated (Marynowski *et al.*, 2007; Gedl *et al.*, 2012). Further decomposition of organic matter, exposed to oxygenated waters, was possible until the wood fragments were buried under younger sediments. Alternatively, an anoxic microenvironment could have separated the organic remains from well-oxygenated pore waters, owing to intense biodegradation of wood fragments and local oxygen depletion around them. Even though the rate of sedimentation in the basin was uneven (Majewski, 2000; Zatoń *et al.*, 2011; Leonowicz, 2016), it could not be responsible for the differences in preservation of wood fragments as the concretions were sampled from the same horizon P. Following deposition and shallow burial, the wood fragments entered anaerobic conditions within the sediment. The permeability of fine-grained sediments is low, compared to that of coarse-grained deposits, nevertheless at early-diagenetic stage, up to 10 m in depth, where iron carbonate concretions are commonly formed, oxygen diffusion from pore waters is typically effective (Curtis *et al*., 1986; Wetzel and Bojanowski, 2022). However, diffusing oxygen also would have become quickly consumed during further decomposition of the larger organic remains, buried in the sediment column. Relatively rapid depletion of oxygen in microenvironments around individual organic particles induced iron and sulphate reduction, due to microbial activity (Ahmed and Lin, 2017). During microbial decomposition, hydrogen sulphide, carbon dioxide and carbonate ions were produced (Majewski, 2000), according to the following reaction:

$$SO_4^{2-} + \text{organic matter} \rightarrow H_2S + HCO_3^- + CO_2 + H^+ \quad [1]$$

Sulphate-reducing microbes are not the only microorganisms, which may lead to the decomposition of organic matter and ion differentiation within the sediment. Iron-reducing microbes behave in a similar way (Ahmed and Lin, 2017; Ebrahiminezhad *et al.*, 2017). This type of microorganism receives metabolic energy from the decay of organic matter, coupled with iron reduction. During that process, an electron is transferred from organic matter to ferric ion (Fe^{3+}), according to the reaction (Ahmed and Lin, 2017):

$$Fe^{3+} + \text{organic matter} \rightarrow Fe^{2+} + HCO_3^- + CO_2 + H^+ \quad [2]$$

The occurrence of microbial organisms, organic carbon, and ferric ions, commonly accumulated among the surrounding sediments in anoxic conditions, led to the reduction of ferric ions (Fe^{3+}) to ferrous ions (Fe^{2+}) (Fig. 8; Ahmed and Lin, 2017). The presence of decomposing organic matter had significant importance for siderite crystallization. The occurrence of siderite usually indicates the development of one of the two environments, suboxic or anoxic conditions, induced by microbial decomposition of organic matter, or methanogenesis, resulting from microbial activity (Curtis *et al*., 1986; Coleman, 1993). The formation of iron carbonate concretions in a methanogenesis zone is distinguishable by the heavy $\delta^{13}C$ composition of carbonates (Pye *et al.*, 1990; Coleman *et al*., 1993; Bojanowski and Clarkson, 2012). $\delta^{13}C$ measurements, conducted on siderite samples from the cortex of the analysed concretions, displayed the negative values: -9.5‰, -9‰ and -7.8‰, what indicates rather light $\delta^{13}C$ composition. Therefore, probably it was not

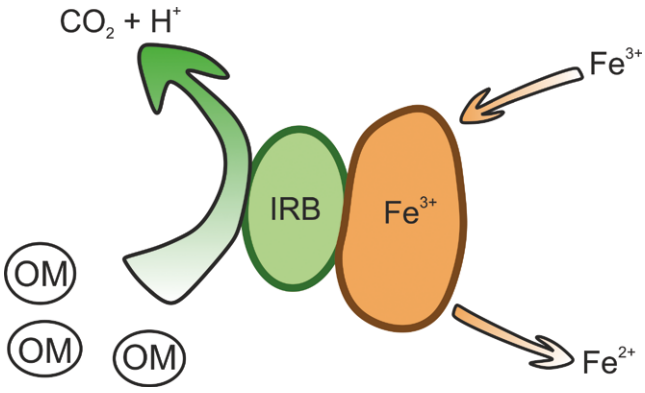

Fig. 8 Scheme of organic matter oxidation and iron reduction mediated by iron- reducing bacteria. OM – organic matter; IRB – iron-reducing bacteria. Adapted after Esther *et al.*, (2015).

methanogenesis that induced siderite crystallization around the wood fragments (Curtis *et al.*, 1986; Coleman, 1993; Bojanowski and Clarkson, 2012). The composition of stable carbon isotopes from the cortex of concretions is characteristic for ^{13}C-depleted bicarbonate, released by iron- or sulphate-reducing microbes during the oxidation of organic matter in oxygen – deficient conditions (Raiswell, 1988; Mozley and Carothers, 1992; Bojanowski and Clarkson, 2012). The decomposition of organic matter by iron reduction yields more energy than sulphate reduction, therefore in an anoxic environment with abundant accumulation of OM and available Fe^{3+} and sulphate ions, an iron reduction zone will develop preferentially before sulphate reduction within the sediment (Chapelle and Lovley, 1992; Bethke *et al.*, 2011). Intensive decomposition of OM around wood fragments probably could lead to an iron deficit in highly anoxic microenvironments, where sulphate reduction would predominate. That could induce an increase in alkalinity and therefore contribute to precipitation of siderite around wood fragments (Lin *et al.*, 2020). This is analogous to the model proposed by Bojanowski and Clarkson (2012) for siderite concretions precipitated around faecal pellets. The most significant difference is that they report methanogenic microenvironments developed in the zone of sulphate reduction. Siderite crystallization ensued from the synthesis reaction of bicarbonate (HCO_3^-) and ferrous ions (Fe^{2+}), at the stage of early diagenesis (Fig. 9).

[3] $$Fe^{2+} + HCO_3^- \rightarrow FeCO_3 + H^+$$

Plant fragments acted as initial nuclei and provided a reducing factor. Siderite cemented sediment with organic remains, so that the entire material could be enclosed within the concretions (Bojanowski and Clarkson, 2012). The ellipsoidal and usually flattened shape of the concretions

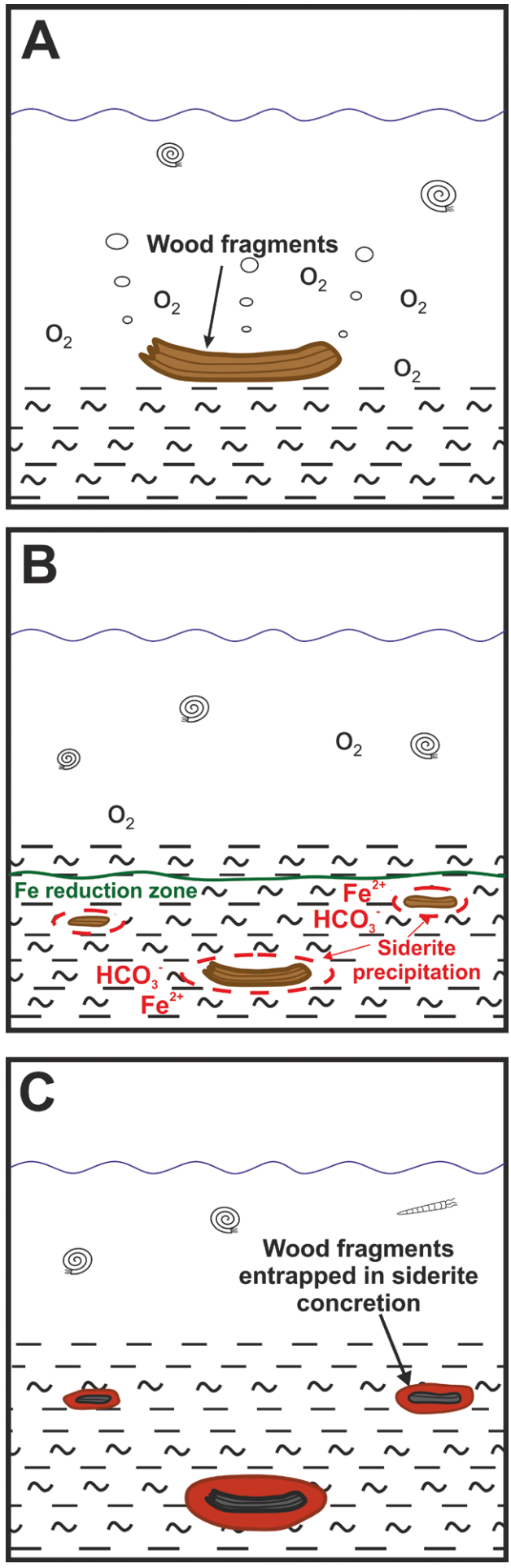

Fig. 9. Formation model of siderite concretions with entrapped wood fragments. **A.** Oxidation of organic matter at the bottom of the sea. **B**. Beginning of siderite precipitation around wood fragments. **C**. Entrapment of organic matter inside the concretions.

analysed reflects permeability anisotropy of the sediment. The flow of pore waters and the delivery of ions were considerably more effective horizontally than in a vertical direction. For this reason, the growth of concretions developed preferentially in the bedding plane (Sellés-Martínez, 1996; Witkowska, 2012). The elongated shape of the wood fragments also could have exerted influenced the final appearance of the concretions, as they acted as the initial nuclei for siderite precipitation.

Ions produced during the decomposition of organic matter became a source of sulphide crystallization and influenced mineral differentiation between the concretions. The most common amongst them is pyrite, which occurred through synthesis reactions of sulphide ions (S^{2-}, from H_2S dissociation) with abundant ferrous ions (Fe^{2+}; Wilkin and Barnes, 1997; Zatoń *et al.*, 2008). With the migration of pore waters in a sediment, the ions of Zn^{2+} and Pb^{2+} could be delivered to the system, leading to the crystallization of sphalerite and galena in the concretions.

The development of early-diagenetic, microbial decay of organic matter and siderite cementation also is determined by the sedimentation rate in a basin (Raiswell, 1988; Taylor and Macquarker, 2000). Conditions promoting siderite crystallization require relative stability of the diagenetic zones in a sediment column. Fluctuations in the rate of sedimentation or episodes of reduced sediment supply may have led to the establishment of those diagenetic zones within the sediment column. Therefore, siderite crystallization around wood fragments might have been developed in stable redox conditions (Coleman, 1993; Witkowska, 2012).

CONCLUSIONS

Analysed siderite concretions from the Gnaszyn clay-pit enclose preserved wood fragments. The organic matter in the wood structures was characterized as immature kerogen, containing low amounts of hydrogen and relatively high quantities of oxygen. According to the depositional environment and maceral composition, it is presumed that the original kerogen belonged to type III, but the extended time of decomposition and oxygenation, as well as significant amounts of carbonates dominated by siderite, drove the kerogen into the kerogen type IV window on the basis of RE analyses.

Organic fragments from the higher plants reveal variability in preservation of the cellular structure. While the majority of the fragments display well-preserved wood structures, dominated by textinite and ulminite, with little to no mechanical deformation, some of the fragments or parts of the fragments show degradation of the cellular structure and mechanical compaction. The variability of structure preservation is probably linked to different degrees of biodegradation encountered in oxic terrestrial environments before deposition at the bottom of the basin. After the final burial of wood fragments and the isolation of them from well-oxygenated basin waters, organic decay was facilitated by microbes reducing iron and sulphates. Progressive organic decay provided bicarbonate and could contribute to lowering of the pH, until siderite precipitation occurred. Siderite crystallization occurred in microenvironments surrounding the organic particles, as a result of the synthesis reaction of bicarbonate ions (HCO_3^-) and ferrous ions (Fe^{2+}), delivered by microbes during iron and sulphate reduction processes. In this sequence of events, individual organic particles acted as nuclei for concretionary growth. The crystallization of siderite cement in clay material with wood fragments occurred during early diagenesis at shallow burial, which prevented the wood fragments from undergoing further mechanical deformation and chemical alteration. The characteristic, flattened shape of the iron carbonate concretions developed as a result of anisotropy of sediment permeability, which favoured growth along the bedding planes.

Acknowledgements

The fieldwork conducted in this project was possible thanks to permission from the Wienerberger Gnaszyn, belonging to the Wienerberger Group. We thank W. Drzewicki, M. Kochel, P. Matz, M. Prell and J. Stachoń (University of Wrocław), B. Marciniak-Maliszewska and P. Jokubauskas (University of Warsaw), and B. Massalska (Polish Geological Institute – National Research Institute) for their technical and analytical assistance. Thanks go to A. Solecki (University of Wrocław) for discussions about isotopic data. We thank reviewers M. Bojanowski and H. Claes as well as Associate Editor B. Budzyń for their valuable remarks, which helped to improve the manuscript. This paper was prepared thanks to the internal project, "Petrochemical properties of organic matter from the Middle Jurassic siderite horizon in the Gnaszyn area", supported by the Institute of Geological Sciences, University of Wrocław.

REFERENCES

Ahmed, M. & Lin, L., 2017. Ferric reduction in organic matter oxidation and its applicability for anaerobic wastewater treatment: a review and future aspects. *Reviews in Environmental Science and Bio/Technology*, 16: 273–287.

Alyousuf, T., Algharbi, W., Algeer, R. & Samsudin, A., 2011. Source rock characterization of the Hanifa and Tuwaiq Mountain formations in the Arabian Basin, based on Rock-Eval Pyrolysis and the Modified Delta Log R Method. [*Paper presented at the SPE/DGS Saudi Arabia Section Technical Symposium and Exhibition, Al-Khobar, Saudi Arabia, May 2011*], paper, SPE-149119-MS, published: 15.05.2011, doi: https://doi.org/10.2118/149119-MS

Bassler, R. S., 1908. The formation of geodes with remarks on the silicification of fossils. *Proceedings of the United States National Museum*, 35: 133–154.

Behar, F., Beaumont, V., Penteado, H. L. & De, B., 2001. Rock-Eval 6 technology: Performances and developments technologie Rock-Eval 6: performances et développements. *Oil and Gas Science and Technology*, 56: 111–134.

Bethke, C. M., Sanford, R. A., Kirk, M. F., Jin, Q. & Flynn, T. M., 2011. The thermodynamic ladder in geomicrobiology. *American Journal of Science*, 311: 183–210.

Blome, C. D. & Albert, N. R., 1985. Carbonate concretions: An ideal sedimentary host for microfossils. *Geology*, 13: 212–215.

Bojanowski, M. J., Barczuk, A. & Wetzel, A., 2014. Deep-burial alteration of early-diagenetic carbonate concretions formed in Palaeozoic deep-marine greywackes and mudstones

(Bardo Unit, Sudetes Mountains, Poland). *Sedimentology*, 61: 1211–1239.

Bojanowski, M. J. & Clarkson, E. N. K., 2012. Origin of siderite concretions in microenvironments of methanogenesis developed in a sulfate reduction zone: an exception or a rule? *Journal of Sedimentary Research*, 82: 585–598.

Ceglarska-Stefańska, G., 1994. Petrografia węgla kamiennego. In: Czapliński, A. (ed.), *Węgiel kamienny*. Wydawnictwa Akademii Górniczo-Hutniczej im. Stanisława Staszica w Krakowie, Kraków, pp. 41–55. [In Polish.]

Chapelle, F. H. & Lovley, D. R., 1992. Competitive exclusion of sulfate reduction by Fe(III)-reducing bacteria: A mechanism for producing discrete zones of high-iron ground water. *Ground Water*, 30: 29–36.

Coleman, M. L., 1993. Microbial processes: control on the shape and composition of carbonate concretions. *Marine Geology*, 113: 127–140.

Coleman, M. L., Hedrick, D. B., Lovley, D. R., White, D. C. & Pye, K., 1993. Reduction of Fe(III) in sediments by sulphate-reducing bacteria. *Nature,* 361: 436–438.

Coleman, M. L. & Raiswell, R., 1993. Microbial mineralization of organic matter: Mechanisms of self-organization and inferred rates of precipitation of diagenetic minerals: *Royal Society of London, Philosophical Transactions*, 344 (A): 69–87.

Cotroneo, S., Schiffbauer, J. D., McCoy, V. E., Wortmann, U. G., Darroch, S. A. F., Peng, Y. & Laflamme, M., 2016. A new model of the formation of Pennsylvanian iron carbonate concretions hosting exceptional soft-bodied fossils in Mazon Creek, Illinois. *Geobiology*, 14: 543–555.

Curtis, C. D., Coleman, M. L. & Love, L. G., 1986. Pore water evolution during sediment burial from isotopic and mineral chemistry of calcite, dolomite and siderite concretions. *Geochimica et Cosmochimica Acta*, 50: 2321–2334.

Dadlez, R., Marek, S. & Pokorski, J. (eds.), 2000. *Geological Map of Poland without Cenozoic Deposits, Scale 1:1000000.* Polish Geological Institute – National Research Institute, Warszawa. [In Polish.]

Daly, R. A., 1900. The calcareous concretions of Kettle Point, Lambton count, Ontario. *The Journal of Geology*, 8: 135.

Dayczak-Calikowska, K., 1997. Jura środkowa: sedymentacja, paleogeografia i paleotektonika. In: Marek, S. & Pajchlowa, M. (eds.), *Epikontynentalny perm i mezozoik w Polsce*. *Prace Państwowego Instytutu Geologicznego*, 153: 269–282. [In Polish.]

Dayczak-Calikowska, K. & Kopik, J., 1973. Jura środkowa. In: *Budowa geologiczna Polski, Tom 1, Stratygrafia, cz. 2, Mezozoik.*. Wydawnictwa Geologiczne, Warszawa, pp. 237–324. [In Polish.]

Dellisanti, F., Pini, G. A. & Baudin, F., 2010. Use of Tmax as a thermal maturity indicator in orogenic successions and comparison with clay mineral evolution. *Clay Minerals*, 45: 115–130.

Dembicki, H., Jr., 2017. *Practical Petroleum Geochemistry for Exploration and Production*. Elsevier, 342 pp.

Dembicz, K. & Praszkier, T., 2003. Zróżnicowanie litofacjalne osadów keloweju w rejonie Zawiercia. *Volumina Jurassica*, 1: 53–58. [In Polish.]

Ebrahiminezhad, A., Manafi, Z., Berenjian, A., Kianpour, S. & Ghasemi, Y., 2017. Iron-reducing bacteria and iron nanostructures. *Journal of Advanced Medical Sciences and Applied Technologies*, 3: 9–16.

Esther, J., Sukla, L. B., Pradhan, N. & Panda, S., 2015. Fe (III) reduction strategies of dissimilatory iron reducing bacteria. *Korean Journal of Chemical Engineering*, 32: 1–14.

Feldman-Olszewska, A., 1997. Depositional architecture of the Polish epicontinental Middle Jurassic basin. *Geological Quarterly*, 41: 491–508.

Feldman-Olszewska, A., Pieńkowski, G. & Wierzbowski, A., 2017. Mapy miąższości skał w podziale na systemy stratygraficzne – jura. In: Nawrocki, J. & Becker, A. (eds), *Atlas geologiczny Polski*. Państwowy Instytut Geologiczny – Państwowy Instytut Badawczy, Warszawa, pp. 72–73. [In Polish.]

Gautier, D. L., 1982. Siderite concretions: indicator of early diagenesis in the gammon shale (Cretaceous). *Journal of Sedimentary Petrology*, 52: 859–871.

Gedl, P., Kaim, A., Leonowicz, P., Boczarowski, A., Dudek, T., Kędzierski, M., Rees, J., Smoleń, J., Szczepanik, P., Sztajner, P., Witkowska, M. & Ziaja, J., 2012. Palaeoenvironmental reconstruction of Bathonian (Middle Jurassic) ore-bearing clays at Gnaszyn, Kraków-Silesia Homocline, Poland. *Acta Geologica Polonica*, 62: 463–484.

Hackley, P. C., Araujo, C. V., Borrego, A. G., Bouzinos, A., Cardott, B. J., Cook, A.C., Eble, C., Flores, D., Gentzis, T., Gonçalves, P. A., Mendonça Filho, J. G., Hámor-Vidó, M., Jelonek, I., Kommeren, K., Knowles, W., Kus, J., Mastalerz, M., Menezes T. R., Newman, J., Oikonomopoulos, J. K., Pawlewicz, M., Pickel, W., Potter, J., Ranasinghe, P., Read, H., Reyes, J., De La Rosa Rodriguez, G., de Souza, I. V. A. F., Suárez-Ruiz, I., Sýkorová I. & Valentine, B. J., 2015. Standardization of reflectance measurements in dispersed organic matter: Results of an exercise to improve interlaboratory agreement. *Marine and Petroleum Geology*, 59: 22–34.

Haisig, J., 2011. *Objaśnienia do Mapy Geologicznej Polski w skali 1:200000. Arkusz 57, Częstochowa.* Państwowy Instytut Geologiczny – Państwowy Instytut Badawczy, Warszawa, 61 pp. [In Polish.]

Haisig, J. & Wilanowski, S., 2008. *Objaśnienia do reambulowanej Mapy Geologicznej Polski w skali 1:200000. Arkusz 56, Kluczbork*. Państwowy Instytut Geologiczny, Warszawa, 61 pp. [In Polish.]

Janssen, K., Mähler, B., Rust, J., Bierbaum, G. & McCoy, V. E., 2022. The complex role of microbial metabolic activity in fossilization. *Biological Reviews*, 97: 449–465.

Killops, S. & Killops V., 2005. *Introduction to Organic Geochemistry, Second Edition*. Blackwell Publishing Ltd, 393 pp.

Kruszewska, K. & Dybova-Jachowicz, S., 1997. *Zarys petrologii węgla. Skrypty Uniwersytetu Śląskiego*, 525, 200 pp. Wydawnictwo Uniwersytetu Śląskiego, Katowice. [In Polish.]

Kutek, J., 1994. Jurassic tectonic events in south-eastern cratonic Poland. *Acta Geologica Polonica*, 44: 167–222.

Labus, M., Kierat, M., Matyasik, I., Spunda, K., Kania, M., Janiga, M., Bieleń, W., 2019. The use of compiled thermal methods in the characteristics of source rocks on the example of menilite beds. *Nafta-Gaz*, 2: 67–76. [In Polish, with English summary.]

Lafargue, E., Marquis, F. & Pillot, D., 1998. Rock-Eval 6 applications in hydrocarbon exploration, production and soils contamination studies. *Oil and Gas Science and Technology*, 53: 421–437.

Lamlom, S. H. & Savidge, R. A., 2003. A reassessment of carbon content in wood: variation within and between 41 North American species. *Biomass and Bioenergy*, 25: 381-388.

Leonowicz, P., 2013. The significance of mudstone fabric combined with palaeoecological evidence in determining sedimentary processes – an example from the Middle Jurassic of southern Poland. *Geological Quarterly*, 57: 243–260.

Leonowicz, P., 2015a. Storm-influenced deposition and cyclicity in a shallow-marine mudstone succession – example from the Middle Jurassic ore-bearing clays of the Polish Jura (southern Poland). *Geological Quarterly*, 59: 325–344.

Leonowicz, P. 2015b. Ichnofabrics of shallow-marine mudstone, the result of changing environmental conditions: an example from the Middle Jurassic ore-bearing clay from southern Poland. *Facies*, 61: 11, https://doi.org/10.1007/s10347-015-0438-4.

Leonowicz, P., 2016. Nearshore transgressive black shale from the Middle Jurassic shallow-marine succession from southern Poland. *Facies,* 62: 16.

Lin, C. Y., Turchyn, A. V., Krylov, A. & Antler, G., 2020. The microbially driven formation of siderite in salt marsh sediments. *Geobiology*, 18: 207–224.

Majewski, W., 2000. Middle Jurassic concretions from Częstochowa (Poland) as indicators of sedimentation rates. *Acta Geologica Polonica*, 50: 431–439.

Marynowski, L., Zatoń, M., Simoneit, R. T. Bernd, Otto, A., Jędrysek M. O., Grelowski C. & Kurkiewicz, S., 2007. Compositions, sources and depositional environments of organic matter from the Middle Jurassic clays of Poland. *Applied Geochemistry*, 22: 2456–2485.

Matyja, B. A. & Wierzbowski, A., 2000. Ammonites and stratigraphy of the uppermost Bajocian and Lower Bathonian between Częstochowa and Wieluń, Central Poland. *Acta Geologica Polonica*, 50: 191–209

Matyja, B. A. & Wierzbowski, A., 2003. Biostratygrafia amonitowa formacji częstochowskich iłów rudonośnych (najwyższy bajos – górny baton) z odsłonięć w Częstochowie. *Tomy Jurajskie*, 1: 3–6. [In Polish.]

McCarthy, K., Rojas, K., Palmowski, D., Peters, K. & Stankiewicz, A., 2011. Basic petroleum geochemistry for source rock evaluation. *Oilfield Review*, 23: 32–43.

McCrea, J. M., 1950. The isotopic chemistry of carbonates and a paleotemperature scale. *Journal of Chemical Physics*, 18: 849–857.

Mozley, P. S., 1996. The internal structure of carbonate concretions in mudrocks: a critical evaluation of the conventional concentric model of concretion growth. *Sedimentary Geology*, 103: 85–91.

Mozley, P. S. & Carothers, W. W., 1992. Elemental and isotopic composition of siderite in the Kuparuk Formation, Alaska: effect of microbial activity and water/sediment interaction on early pore-water chemistry. *Journal of Sedimentary Petrology*, 62: 681–692.

Osika, R. & Cieśla, E., 1990. Sedimentary ores. In: Osika, R. (ed.), *Geology of Poland vol. VI, Mineral Deposits*. Wydawnictwa Geologiczne, Warszawa, pp. 137–147.

Peters, K. E., 1986. Guidelines for evaluating petroleum source rock using programmed pyrolysis. *American Association of Petroleum Geologists Bulletin*, 70: 318–329.

Peters, K. E., Curry, D. J. & Kacewicz, M., 2012. An overview of basin and petroleum system modeling: Definitions and Concepts. In: Peters, K. E., Curry, D. J. & Kacewicz, M., (eds.), *Basin Modeling: New Horizons in Research and Application*. *AAPG Hedberg Series*, 4: 1–16.

Pieńkowski, G., Schudack, M. E., Bosák, P., Enay, R., Feldman-Olszewska, A., Golonka, J., Gutowski, J., Herngreen, G. F. W., Jordan, P., Krobicki, M., Lathuiliere, B., Leinfelder, R. R., Michalík, J., Mönnig, E., Noe-Nygaard, N., Pálfy, J., Pint, A., Rasser, M. W., Reisdorf, A. G., Schmid, D. U., Schweigert, G., Surlyk, F., Wetzel, A. & Wong, T. E., 2008. Jurassic. In: McCann, T. (ed.), *The Geology of Central Europe. Volume 2: Mesozoic and Cenozoic.* Geological Society of London, pp. 823–922.

Pouchou, J. L. & Pichoir, J., 1984. A new model for quantitative X-ray microanalysis. *Recherche Aérospatiale* 3: 167–192.

Pye, K., Dickson, J. A. D., Schiavon, N., Coleman, M. L. & Cox, M., 1990. Formation of siderite-Mg-calcite-iron sulphide concretions in intertidal marsh and sandflat sediments, north Norfolk, England. *Sedimentology*, 37: 325–343.

Raiswell, R., 1988. Chemical model for the origin of minor limestone-shale cycles by anaerobic methane oxidation. *Geology*, 16: 641–644.

Raiswell, R. & Fisher, Q. J., 2000. Mudrock- hosted carbonate concretions: a review of growth mechanisms and their influence on chemical and isotopic composition. *Journal of the Geological Society*, 157: 239–251.

Ratajczak, T. & Korona, W., 2000. Mineralogical-chemical and technological characteristics of mineral matter from dumps after mining of iron ores the Częstochowa region (Central Poland). *Przegląd Geologiczny*, 48: 607–616. [In Polish, with English summary.]

Richardson, W. A., 1919. On the origin of septarian structure. *Mineralogical Magazine*, 56: 327–337.

Roberts, J. A., Kenward, P. A., Fowle, D. A., Goldstein, R. H., González, L. A. & Moore, D. S., 2013. Surface chemistry allows for abiotic precipitation of dolomite at low temperature. *Proceedings of the National Academy of Sciences*, 110: 14540–14545.

Różycki, S. Z., 1953. Górny dogger i dolny malm Jury Krakowsko-Częstochowskiej. *Prace Instytutu Geologicznego*, 17: 1–351. [In Polish.]

Sellés-Martínez, J., 1996. Concretion morphology, classification and genesis. *Earth-Science Reviews*, 41: 177–210.

Stupnicka, E. & Stempień-Sałek, M., 2016. *Geologia regionalna Polski*. Wydawnictwa Uniwersytetu Warszawskiego, Warszawa, 342 pp. [In Polish.]

Szczepanik, P., Witkowska, M. & Sawłowicz, Z., 2007. Geochemistry of Middle Jurassic mudstones (Kraków-Częstochowa area, southern Poland): interpretation of the depositional redox conditions. *Geological Quarterly*, 51: 57–66.

Szczepańska, M. & Witkowska, M., 2007. Surowce ilaste ceramiki budowlanej w dawnych ośrodkach wydobycia rud żelaza. *Warsztaty 2007 z cyklu: Zagrożenia naturalne w górnictwie. Materiały Warsztatów*, pp. 153–163. [In Polish.]

Tarr, W. A., 1921. Syngenetic origin of concretions in shale. *Bulletin of the Geological Society of America*, 32: 373–384.

Taylor, K. G. & Macquarker, J. H. S., 2000. Early diagenetic pyrite morphology in a mudstone-dominated succession: the Lower Jurassic Cleveland Ironstone Formation, eastern England. *Sedimentary Geology,* 131: 77–86.

Tissot, B., Durand, B., Espitalié, J. & Combaz, A., 1974. Influence of nature and diagenesis of organic matter in formation of petroleum. *AAPG Bulletin,* 58: 499–506.

Wetzel, A. & Bojanowski, M., 2022. Radish concretions grown in mud during compaction. *Sedimentology*, 69: 750–774.

Wierzbowski, H., 2015. Seawater temperatures and carbon isotope variations in central European basins at the Middle–Late Jurassic transition (Late Callovian–Early Kimmeridgian). *Palaeogeography, Palaeoclimatology, Palaeoecology*, 440: 506–523.

Wierzbowski, H., Dembicz, K. & Praszkier, T., 2009. Oxygen and carbon isotope composition of Callovian-Lower Oxfordian (Middle-Upper Jurassic) belemnite rostra from central Poland: A record of a Late Callovian global sea-leve rise? *Palaeogeography, Palaeoclimatology, Palaeoecology*, 283: 182–194.

Wilkin, R. T. & Barnes, H. L., 1997. Formation processes of framboidal pyrite. *Geochimica et Cosmochimica Acta*, 61: 323–339.

Witkowska, M., 2012. Palaeoenvironmental significance of iron carbonate concretions from the Bathonian (Middle Jurassic) ore-bearing clays at Gnaszyn, Kraków-Silesia Homocline, Poland. *Acta Geologica Polonica*, 62: 307–324.

Yeboah, D., Burton, A. J., Storer, A. J. & Opuni-Frimpong, E., 2014. Variation in wood density and carbon content of tropical plantation tree species from Ghana. *New Forests* 45: 35–52.

Zatoń, M., Machocka, S., Wilson, M. A., Marynowski, L. & Taylor, P. D., 2011. Origin and paleoecology of Middle Jurassic hiatus concretions from Poland. *Facies*, 57: 275–300.

Zatoń, M., Marynowski, L., Szczepanik, P., Bond, D. P. & Wignall, P. B., 2009. Redox conditions during sedimentation of the Middle Jurassic (Upper Bajocian–Bathonian) clays of the Polish Jura (south-central Poland). *Facies*, 55: 103–114.

Zatoń, M., Rakociński, M. & Marynowski, L., 2008. Pyrite framboids as paleoenvironmental indicators. *Przegląd Geologiczny*, 56: 158–164. [In Polish, with English summary.]